Nanoscale

PAPER

View Article Online
View Journal | View Issue

Open Access Article. Published on 12 June 2015. Downloaded on 12/5/2025 1:54:21 AM.
This article is licensed under a Creative Commons Attribution 3.0 Unported Licence.

Cite this: *Nanoscale*, 2015, **7**, 12085

Surfactant-free Gd^{3+}-ion-containing carbon nanotube MRI contrast agents for stem cell labeling†

Ayrat Gizzatov,[a] Mayra Hernández-Rivera,[a] Vazrik Keshishian,[a] Yuri Mackeyev,[a] Justin J. Law,[a] Adem Guven,[a] Richa Sethi,[a] Feifei Qu,[b] Raja Muthupillai,[b] Maria da Graça Cabreira-Hansen,[c] James T. Willerson,[c] Emerson C. Perin,[c] Qing Ma,[d] Robert G. Bryant[e] and Lon J. Wilson*[a]

Received 1st April 2015,
Accepted 5th June 2015

DOI: 10.1039/c5nr02078f

www.rsc.org/nanoscale

There is an ever increasing interest in developing new stem cell therapies. However, imaging and tracking stem cells *in vivo* after transplantation remains a serious challenge. In this work, we report new, functionalized and high-performance Gd^{3+}-ion-containing ultra-short carbon nanotube (US-tube) MRI contrast agent (CA) materials which are highly-water-dispersible (*ca.* 35 mg ml^{-1}) without the need of a surfactant. The new materials have extremely high T_1-weighted relaxivities of 90 (mM s)$^{-1}$ per Gd^{3+} ion at 1.5 T at room temperature and have been used to safely label porcine bone-marrow-derived mesenchymal stem cells for MR imaging. The labeled cells display excellent image contrast in phantom imaging experiments, and TEM images of the labeled cells, in general, reveal small clusters of the CA material located within the cytoplasm with 10^9 Gd^{3+} ions per cell.

Introduction

Magnetic resonance imaging (MRI) is one of the most frequently-used noninvasive diagnostic tools in the clinic. Often, MRI contrast agents (CAs) are used to enhance the sensitivity of the imaging technique by interacting with the water molecule protons within the body, to reduce the T_1 spin-lattice (T_1) and spin–spin (T_2) relaxation times of the proton nuclear spin excited state, thereby producing greater image contrast. CAs are valuable for various applications such as the imaging of tissue which is difficult to distinguish by conventional MRI, tracking the delivery of nanoparticles, and labeling cells for possible *in vivo* monitoring.[1–9]

CAs are usually chemical compounds containing paramagnetic (Gd^{3+}, Mn^{2+}) chelate compounds with larger effect on T_1 shortening or superparamagnetic materials like Fe_3O_4 with larger effect on T_2 shortening. However, T_1 for a soft tissue within the body is significantly longer than T_2.[10] Gd^{3+}-ion-based CAs, which primarily affect T_1 values, can therefore produce larger differences in relaxation times than Fe_3O_4 based agents, which primarily affect T_2 values. Thus, Gd^{3+}-ion based-agents are favored because they can be more easily detected against image backgrounds.

In the past decade, the development of various Gd^{3+}-ion-based magnetic nanomaterials has led to many advances in MRI CAs design.[11,12] In particular, ultra-short single-walled carbon nanotubes (US-tubes) and graphene-based MRI CAs have been shown to dramatically increase the efficacy of Gd^{3+} ions in reducing the relaxation time of excited proton nuclear spins, resulting in better image contrast.[13–15] Gd^{3+}-ion-containing US-tubes (Gadonanotubes or GNTs) and related materials are especially promising MRI CA candidates due to their high relaxivity and ability to traverse the cellular membrane.[4] This ability to function as an intracellular label leads to many potential imaging applications which are not possible with conventional macrocyclic gadolinium chelates which are limited to the vasculature. One such application for these materials is in stem cell labeling and tracking. Even though many strategies for tracking stem cells have been developed, such as Fe_3O_4 nanoparticles for MRI, and radiolabeling with

[a]Department of Chemistry, Richard E. Smalley Institute for Nanoscale Science and Technology, Rice University, 6100 Main Street, Houston, TX 77251-1892, USA. E-mail: durango@rice.edu
[b]Department of Radiology, St. Luke's Episcopal Hospital, MC 2-270, 6720 Bertner Avenue, Houston, TX 77030-2697, USA
[c]Stem Cell Center, Texas Heart Institute at St. Luke's Episcopal Hospital, MC 2-255, 6720 Bertner Avenue, Houston, TX 77225-0345, USA
[d]DND-CAT, Northwestern Synchrotron Research Center at the Advanced Photon Source, 9700 S. Cass Avenue, Argonne, IL 60439, USA
[e]Department of Chemistry, University of Virginia, P.O. Box 400319, Charlottesville, VA 22904-4319, USA

†Electronic supplementary information (ESI) available: NMRD profiles, the Fourier transforms of the EXAFS data, EXAFS curve fitting data, cell viability data. See DOI: 10.1039/c5nr02078f

Open Access Article. Published on 12 June 2015. Downloaded on 12/5/2025 1:54:21 AM.
This article is licensed under a Creative Commons Attribution 3.0 Unported Licence.

positron emission tomography (PET) or single-photon emission computed tomography (SPECT) agents, there still remains a need for new high-performance cell tracking and imaging tools in order to monitor changes in transplanted stem cells *in vivo*.[5,16–20] GNTs are ideal imaging agents for this role, and previous work has shown initial success in this area.[4,6,19]

However, one of the current limitations of GNTs as a cellular label is that, due to the hydrophobic nature of carbon nanotubes, GNTs are prone to aggregate in aqueous media and require addition of surfactant for dispersal. This is, however, not an ideal situation, as surfactant coatings may be removed *in vivo*, resulting in aggregation of the contrast agent within the cell.

In previous work, we reported a method for enhancing water dispersibility of carbon nanotube and similar graphitic materials by covalently attaching benzoic acid groups *via* diazonium-based chemistry.[21] However, when applied to GNTs, the acidic conditions required for initiation of the reaction might result in leaching of Gd^{3+} ions from the US-tubes, effectively eliminating its ability to produce image contrast. It is also not feasible to produce GNTs from US-tubes which have already been functionalized, as access to the interior cavity through the sidewall defects would be hindered and Gd^{3+} ions would likely be loosely coordinated to the carboxylic acid groups which were added to enhance water dispersibility.

In a separate work, we recently reported the use of Gd^{3+} chelates within US-tubes to probe the coordination environment around the Gd^{3+} ion and its influence on the relaxivity of the GNTs.[22] In the synthesis of these materials, we discovered that the use of Gd^{3+} chelate compounds for the internal loading of Gd^{3+} ions into US-tubes resulted in higher Gd^{3+}-ion content in the product compared to the GNTs, allowing for better image contrast. Additionally, the chelation of Gd^{3+} ions prior to encapsulation resulted in a material which was not reliant on pH-dependent lanthanide chemistry for retention of Gd^{3+} ions within the US-tube, and thus, it was more stable under acidic conditions.

In this work, we have applied the diazonium-based functionalization technique to US-tubes filled with Gd^{3+} chelates to produce new, highly-water-dispersible (surfactant free) US-tube-based MRI CAs for applications in preclinical stem cell labeling and tracking. We have also evaluated the MRI performance of these new CAs and employed one of them to safely label and image porcine bone-marrow-derived mesenchymal stem cells (MSCs).

Results and discussion

Three different Gd@US-tube species which contain either Gd^{3+} ions (GNTs), Gd(acetylacetone)$_3$·2H$_2$O chelates (Gd(acac)$_3$·2H$_2$O@US-tubes), or Gd(hexafluoroacetylacetone)$_3$·2H$_2$O chelates (Gd(hfac)$_3$·2H$_2$O@US-tubes) were synthesized as previously reported.[22] The loaded concentration of the Gd^{3+} ions have been determined by inductively-coupled plasma optical emission spectroscopy (ICP-OES) measurements to be 4.4 wt% for GNTs, 7.9 wt% for Gd(acac)$_3$·2H$_2$O@US-tubes, and 4.5 wt% for Gd(hfac)$_3$·2H$_2$O@US-tubes.[22] Characterization of these materials by nuclear magnetic resonance dispersion (NMRD) resulted in similar dispersion profiles (ESI; Fig. S1†). All three materials exhibit profiles characteristic of first coordination sphere water interactions with Gd^{3+} ion coordinated to a high molecular weight and slowly tumbling environment (Fig. S1†). Low-field relaxation is linearly dependent on the log of the Larmor frequency, a signature of dimensionally-restricted diffusion of water protons near paramagnetic centers.[23–25] This paramagnetism has been attributed to carbon-based radicals stabilized by the extended aromatic structure of the US-tubes, as it is present in all samples, including empty US-tubes.[26] Thus, the low-field relaxation arises from diffusion of water on the radical-containing surface of the US-tubes. In contrast, at frequencies above 10 MHz, the electron-spin relaxation time increases with magnetic field, resulting in an increased effective correlation time for electron-nuclear coupling and increased relaxivity from the Gd^{3+} ions. Additionally, Extended X-ray Absorption Fine Structure (EXAFS) measurements at the Gd $L_{2,3}$ edges revealed that upon loading into US-tubes, the Gd^{3+} ion of the Gd^{3+} chelate compounds retains a coordination sphere structure like that of the corresponding bulk materials (three chelates and two water molecules as ligands), demonstrating that the chelates remained intact within the US-tubes (ESI; Fig. S2 and Table S1†). The X-ray absorption near edge structure (XANES) measurements at the Gd L_1 edge also revealed that a similar local symmetry is retained, as well. This is important because the presence of three chelating ligands around each Gd^{3+} ion should help retain the ions within the US-tubes under aqueous solution and biological media challenges.

Each Gd@US-tubes material was then separately functionalized using a previously reported method.[21] However, reaction conditions (see Experimental section) were slightly modified to avoid the presence of a strongly acidic environment so as to prevent leakage of Gd^{3+} ions from the Gd@US-tubes materials (Fig. 1). Gd^{3+}-ion concentrations for the functionalized compounds were also determined by ICP-OES to be 0.5 wt% for the PCP-GNTs, 3.8 wt% for the PCP-Gd(acac)$_3$·2H$_2$O@US-tubes, and 2.5 wt% for the PCP-Gd(hfac)$_3$·2H$_2$O@US-tubes. From previous work,[21] which has also been confirmed in the current

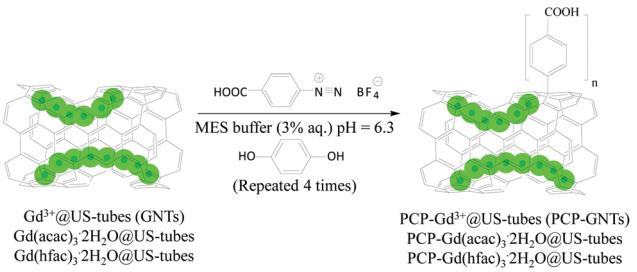

Fig. 1 Functionalization procedure for the three Gd@US-tube materials.

 This journal is © The Royal Society of Chemistry 2015

Open Access Article. Published on 12 June 2015. Downloaded on 12/5/2025 1:54:21 AM.
This article is licensed under a Creative Commons Attribution 3.0 Unported Licence.

work as well (Fig. S3†), it has been established that repeated functionalization for four times of the US-tubes with *p*-carboxyphenyldiazonium (PCP) tetrafluoroborate salt produces up to 50 wt% of covalently-attached benzoic acid moieties to the outer surface of the US-tubes. Therefore a reduction in wt% of Gd^{3+} ions after functionalization of the $Gd(acac)_3{\cdot}2H_2O$@US-tubes from 7.9% to 3.8% and of the $Gd(hfac)_3{\cdot}2H_2O$@US-tubes from 4.5% to 2.5% is consistent with the covalent attachment of the PCP moieties. However, the GNT sample experienced a much greater wt% loss of Gd^{3+} ion: from 4.4% before functionalization to 0.5% after functionalization. This 90 wt% reduction of Gd^{3+} ion for the PCP-GNT sample is attributed to both covalent attachment of the benzoic acid groups, as well as to some leakage of non-chelated Gd^{3+} ions from the US-tubes interior due to the slightly acidic reaction conditions (pH ≈ 4) caused by the addition of *p*-carboxyphenyldiazonium tetrafluoroborate salt during synthesis. In contrast, the Gd^{3+} ions in the PCP-$Gd(acac)_3{\cdot}2H_2O$@US-tube and PCP-$Gd(hfac)_3{\cdot}2H_2O$@US-tube samples are chelated by three acac- or hfac-ligands (and two H_2O molecules), and are therefore more stable to mild acidic conditions.

Relaxivities for the functionalized PCP-Gd^{3+}@US-tubes materials were determined using a bench top relaxometer operating at 1.41 T and RT. Measured relaxivity values are as follows: PCP-GNTs, r_1 = 94 ± 4 (mM s)$^{-1}$; PCP-$Gd(acac)_3{\cdot}2H_2O$@US-tubes, r_1 = 89 ± 4 (mM s)$^{-1}$; and PCP-$Gd(hfac)_3{\cdot}2H_2O$@US-tubes, r_1 = 87 ± 11 (mM s)$^{-1}$. The relaxivity values for the PCP-$Gd(acac)_3{\cdot}2H_2O$@US-tubes and PCP-$Gd(hfac)_3{\cdot}2H_2O$@US-tubes are within the range of the previously reported r_1 values for surfactant (Pluronic® F-108) wrapped $Gd(acac)_3{\cdot}2H_2O$@US-tubes and $Gd(hfac)_3{\cdot}2H_2O$@US-tubes.[22]

To establish their application as MRI CAs, aqueous dispersions of the PCP-GNTs, PCP-$Gd(acac)_3{\cdot}2H_2O$@US-tubes, and PCP-$Gd(hfac)_3{\cdot}2H_2O$@US-tubes, at a concentration of 0.4 mg mL^{-1}, were imaged using a 1.5 T MRI scanner. T_1-weighted MRI phantom images (Fig. 2) acquired using different inversion times (TI) demonstrate that there is a clear visual contrast difference between control (no Gd^{3+}) PCP-US-tubes and PCP-GNTs starting at TI 800 ms, PCP-$Gd(acac)_3{\cdot}2H_2O$@US-tubes at TI 100 ms, and PCP-$Gd(hfac)_3{\cdot}2H_2O$@US-tubes at TI 200 ms. Since r_1 values (per Gd^{3+} ion) of all three Gd^{3+}@US-tubes materials are similar to one another, the greater contrast difference at shorter TI is Gd^{3+}-ion concentration dependent. Therefore, covalently functionalized, highly-water-dispersible PCP-$Gd(acac)_3{\cdot}2H_2O$@US-tubes and PCP-$Gd(hfac)_3{\cdot}2H_2O$@US-tubes are more favorable candidates for applications as MRI CAs when compared to the PCP-GNTs. Hence, cell labeling and the subsequent *in vitro* studies of this work were performed using only PCP-$Gd(acac)_3{\cdot}2H_2O$@US-tubes due to their higher concentration of Gd^{3+} ions encapsulated within the US-tubes, which leads to better MRI performance, as presented in Fig. 2.

To evaluate the performance of the PCP-$Gd(acac)_3{\cdot}2H_2O$@US-tubes (Fig. 3) as an intracellular CA, its toxicity in mesenchymal stem cells (MSCs) was studied using fluorescence-activated cell sorting (FACS) analysis by determining the viability of labeled cells compared to unlabeled control cells. After incubating MSCs with PCP-$Gd(acac)_3{\cdot}2H_2O$@US-tubes (20 μM Gd^{3+}) for 24 h, the uptake of PCP-$Gd(acac)_3{\cdot}2H_2O$@US-tubes by the cells was confirmed and quantified by inductively-coupled plasma mass spectrometry (ICP-MS) analysis. Approximately 10^9 Gd^{3+} ions per cell were successfully taken up, which is about the same concentration of Gd^{3+} ions per cell that can be delivered using Pluronic®-wrapped GNTs, which is an already established intracellular CA.[4] The cytotoxicity studies showed that unlabeled cells were 99.5 ± 0.3% calcein-positive, while PCP-$Gd(acac)_3{\cdot}2H_2O$@US-tube-labeled MSCs exhibited a 98 ± 1% of the calcein signal, showing that the membrane integrity of the cells was not compromised and

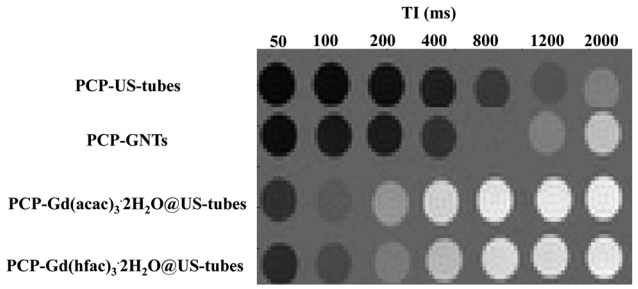

Fig. 2 T_1-weighted MRI phantom images of aqueous dispersion of PCP-US-tubes, PCP-GNTs (0.0127 mM Gd^{3+}), PCP-$Gd(acac)_3{\cdot}2H_2O$@US-tubes (0.0966 mM Gd^{3+}), and PCP-$Gd(hfac)_3{\cdot}2H_2O$@US-tubes (0.0636 mM Gd^{3+}) samples acquired at 1.5 T and RT with different inversion times (TI).

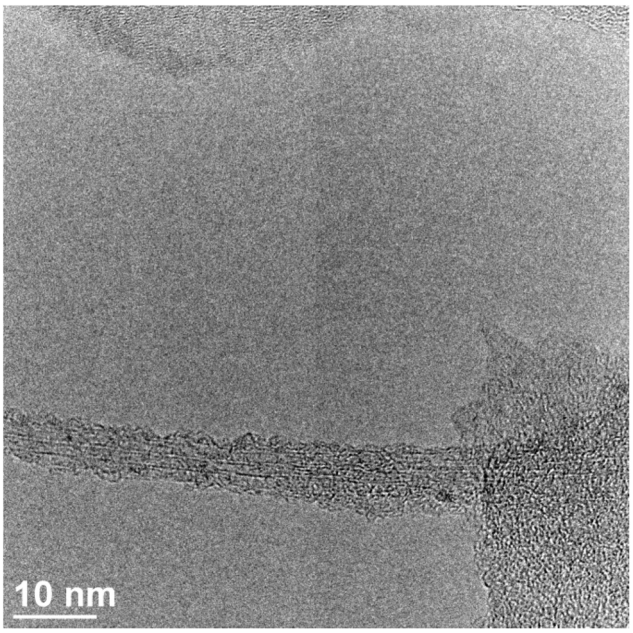

Fig. 3 Transmission electron microscopy image of the bundled PCP-$Gd(acac)_3{\cdot}2H_2O$@US-tubes sample.

Open Access Article. Published on 12 June 2015. Downloaded on 12/5/2025 1:54:21 AM.
This article is licensed under a Creative Commons Attribution 3.0 Unported Licence.

that the cells remained viable after uptake of PCP-Gd(acac)$_3$·2H$_2$O@US-tubes. More details are shown in Fig. S4.†

After demonstrating that PCP-Gd(acac)$_3$·2H$_2$O@US-tubes can be internalized into MSCs to deliver a high concentration of Gd^{3+} ions safely, MRI phantoms of the labeled MSCs were obtained. Ten million and thirty million PCP-Gd(acac)$_3$·2H$_2$O@US-tube-labeled MSCs suspended in 0.5 mL of 0.5% Agar, ten million and thirty million unlabeled control MSCs suspended in 0.5 mL of 0.5% Agar, and pure H$_2$O phantoms were imaged using a 1.5 T MRI scanner. The T_1-weighted MR images in Fig. 4 clearly demonstrate that labeled cells have brighter contrast when compared to unlabeled cells or water phantoms. This is especially observable in the 600–1500 ms TI images. Comparing the two different cell concentrations of PCP-Gd(acac)$_3$·2H$_2$O@US-tubes-labeled MSCs, it can be seen that a greater number of cells produced better T_1 contrast enhancement, as expected due to the higher concentration of Gd^{3+} ions in the sample.

Transmission electron microscopy (TEM) images of PCP-Gd(acac)$_3$·2H$_2$O@US-tube-labeled MSCs in Fig. 5 demonstrate that PCP-Gd(acac)$_3$·2H$_2$O@US-tubes appear as an accumulation of mostly small electron-dense aggregates within the MSCs. In general, the material is not encapsulated within vesicles, but appears to accumulate and aggregate in small clusters within the cytoplasm. From the TEM images it is also apparent that PCP-Gd(acac)$_3$·2H$_2$O@US-tubes do not enter the nucleus. A relatively small number of large PCP-Gd(acac)$_3$·2H$_2$O@US-tube agglomerations per cell were found when compared to previous studies where surfactant-wrapped GNTs were used.[4] While rare, however, a few large clusters were also observed in the present case, like the one showed in Fig. 5A. Since the labeling of the cells using functionalized PCP-Gd(acac)$_3$·2H$_2$O@US-tubes results in approximately the same Gd^{3+}-ion concentration per cell when compared to surfactant-wrapped GNT-labeled cells, it seems that in the present case most of the PCP-Gd(acac)$_3$·2H$_2$O@US-tubes are present as a more dispersed material within the cells. For surfactant-wrapped GNTs, larger aggregates are possibly caused by removal of the surfactant from unfunctionalized GNTs during the cell internalization process. A more in-depth study, however, is needed to properly evaluate the uptake mechanism of these types of materials.

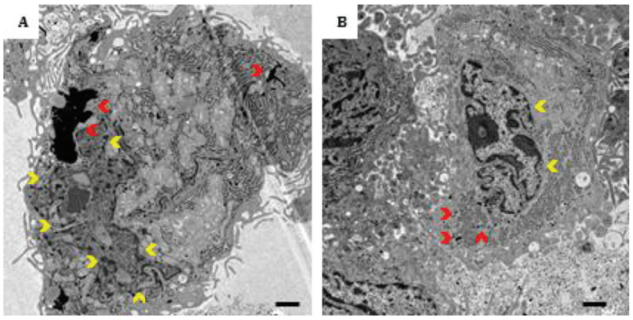

Fig. 5 Representative TEM images of MSCs labeled with PCP-Gd(acac)$_3$·2H$_2$O@US-tubes. Red arrows indicate the intracellular CAs localized in the cytoplasm of the cells, usually in very small clusters, while yellow arrows outline the nucleus. Scale bars = 500 nm.

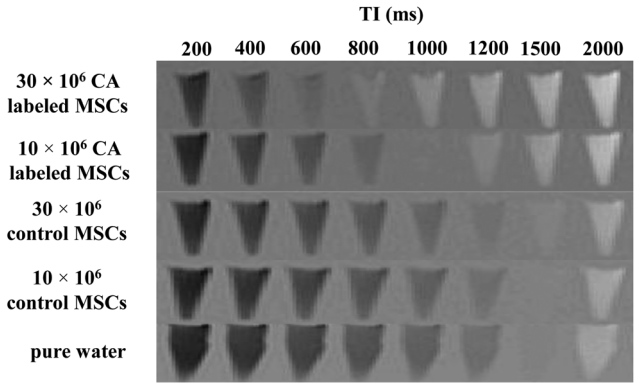

Fig. 4 T_1-weighted MRI phantom images of the samples acquired at 1.5 T and RT as follows: thirty and ten million of PCP-Gd(acac)$_3$·2H$_2$O@US-tube-labeled MSCs, control samples of thirty and ten million of unlabeled MSCs, and pure water. All cell-containing samples are in 0.5% agarose gel.

Conclusions

In summary, this work has demonstrated covalent functionalization of three different Gd@US-tube-based MRI CAs to produce their highly-water-dispersible counterparts: PCP-GNTs, PCP-Gd(acac)$_3$·2H$_2$O@US-tubes, and PCP-Gd(hfac)$_3$·2H$_2$O@US-tubes. The PCP-Gd(acac)$_3$·2H$_2$O@US-tube material can be dispersed in aqueous solution to the extent of approximately 35 mg mL^{-1} without the use of a surfactant. Furthermore, it has been shown that the PCP-Gd(acac)$_3$·2H$_2$O@US-tube CAs can be safely used to internally label pig bone-marrow-derived mesenchymal stem cells (MSCs) to visualize the cells with MRI with potential applications for monitoring transplanted stem cells *in vivo*. Without the need of a surfactant (which can be replaced *in vivo* by proteins and likely other biological entities as well),[27] these new, highly-water-dispersible PCP-Gd(chelate)@US-tube materials also offer the potential to develop a carbon nanotube-based vascular MRI CA for the first time.

Experimental section

Preparation and functionalization of the Gd^{3+}-ion-loaded US-tubes to produce water-dispersible MRI CAs

US-tubes were prepared by a previously established methodology.[28] Briefly, 200 mg of single-walled carbon nanotubes (Carbon Solutions Inc.) were fluorinated using 2% F$_2$ in He gas mixture with a flow rate adjusted to 15 cm^3 min^{-1} along with H$_2$ gas at a flow rate of 10 cm^3 min^{-1} at 125 °C for 2.5 h. The fluorinated product was then heated to 1000 °C for 2 h. under continuous flow of Ar. As produced US-tubes were soni-

 This journal is © The Royal Society of Chemistry 2015

Open Access Article. Published on 12 June 2015. Downloaded on 12/5/2025 1:54:21 AM.
This article is licensed under a Creative Commons Attribution 3.0 Unported Licence.

cated in 200 mL of concentrated HCl for 60 min to remove metal impurities, washed with DI H_2O, dried, and individualized by sonication for 60 min in 200 mL of dry THF and Na^0 (0.5 g). Next, US-tubes were refluxed in 200 mL of 6 M HNO_3 for 15 min, washed with DI H_2O and dried. Loading of the US-tubes with any one of the Gd^{3+}-ion containing agents: (1) $GdCl_3$, (2) Gd(acetylacetone)$_3$·2H_2O (Gd(acac)$_3$·2H_2O), or (3) Gd(hexafluoroacetylacetone)$_3$·2H_2O (Gd(hfac)$_3$·2H_2O) was achieved by 1 h sonication in a 1 mM aqueous solution of $GdCl_3$ to produce Gd@US-tubes or Gadonanotubes (GNTs), or 1 h sonication in a 1 mM solution of Gd(acac)$_3$·2H_2O or Gd(hfac)$_3$·2H_2O in methanol to produce Gd(acac)$_3$·2H_2O@US-tubes and Gd(hfac)$_3$·2H_2O@US-tubes, respectively.[13,22] The products were washed until Gd^{3+} ions could not be detected in the washings (as determined by ICP-OES). The US-tubes-based CAs were then further covalently functionalized using a modified methodology that we have reported previously.[21] Briefly, 40 mg of the Gd^{3+}-ion-containing US-tubes were added to a flask equipped with a magnetic stirring bar and 50 mL of the aqueous 3% 2-(*N*-morpholino)ethanesulfonic acid (MES) buffer solution with the pH adjusted to 6.3. The solution was briefly bath sonicated for 5 min and 500 mg of *p*-carboxyphenyldiazonium (PCP) tetrafluoroborate was added. Reaction was initiated by slow addition of an aqueous hydroquinone solution (3% w/w, excess amount) and left to stir for 30 min until N_2 gas evolution was no longer observed. The product was collected and washed multiple times with DI water and ethanol. The reaction was then repeated three more times to produce highly-water-dispersible, functionalized materials: PCP-GNTs, PCP-Gd(acac)$_3$·2H_2O@US-tubes, and PCP-Gd(hfac)$_3$·2H_2O@US-tubes. The maximum concentration of the PCP-Gd(acac)$_3$·2H_2O@US-tubes in water (*ca.* 35 mg mL^{-1}) was determined by lyophilizing a stable aliquot of a supersaturated solution: briefly, excess of the PCP-Gd(acac)$_3$·2H_2O@US-tubes were dispersed in 1 mL of H_2O and left undisturbed for 24 h, then 250 μL of the supernatant solution was dried and the dry product weighted using a microbalance. The stem-cell-labeling experiments were performed using PCP-Gd(acac)$_3$·2H_2O@US-tubes due to the higher Gd^{3+}-ion concentration (*ca.* 3.8% by weight) within the US-tube material when compared to other two CAs. Additional details are presented in the Discussion section.

Nuclear magnetic resonance dispersion measurements

Nuclear magnetic resonance dispersion data was obtained on a fast field cycling NMR spectrometer (FFC-200, Stelar s.r.l., Mede Italy) in magnetic fields corresponding to proton Larmor frequencies between 0.01 and 30 MHz. Samples were contained in 10 mm diameter glass tubes and maintained at 25 °C using a Stelar VTC90 variable-temperature controller.

Extended X-ray absorption fine structure (EXAFS) measurements

X-ray absorption measurements around the Gd L_3, L_2, L_1 edges were carried out at the 5BM-D beamline of DND-CAT, at the Advanced Photon Source (Argonne, IL). Fine powders of the samples were spread uniformly on strips of Scotch® tape which were folded one time or several times to produce sufficient absorption for measurements in fluorescence mode or in transmission mode. A double crystal Si(111) monochromator was used for energy selection with $\Delta E/E = 1.4 \times 10^{-4}$. The incident X-ray intensity was detuned by 65% of its maximum for harmonic rejection as monitored by an ionization chamber (Oxford, Danfysik). Three such ion chambers were used for measurements in transmission mode. For measurements in fluorescence mode, the Gd L emissions were measured using two 4-element Si-drift vortex detectors (Hitachi, USA).

Relaxometric analysis

Relaxation properties of the Gd^{3+}-ion-loaded US-tube CAs were measured using a Bruker Minispec (mq 60) benchtop relaxometer operating at 1.41 T and 37 °C. The longitudinal (T_1) relaxation times were obtained using an inversion recovery pulse sequence. Gd^{3+}-ion concentration was determined by inductively-coupled plasma optical emission spectroscopy (ICP-OES, using a Perkin-Elmer Inc. Optima 4300 instrumentation). Samples were digested in 26% $HClO_3$ and reconstituted in 5 mL of trace metal-grade 2% $HNO_{3(aq)}$ prior to data collection.

Samples for MR imaging

Phantom MR images of the Gd^{3+}-ion-loaded US-tubes CAs were prepared by taking a 0.4 mg mL^{-1} aqueous dispersion of each sample. T_1 weighted MR images of the samples were then measured using a commercial 1.5 T MRI scanner (Achieva, Philips Medical System, The Netherlands) with an inversion recovery prepared spin echo sequence with the following acquisition parameters: acquired voxel size: 0.94 × 0.94 × 5 mm^3; TR/TE: 10 000 ms /9.76 ms; inversion times (TIs): 50, 100, 200, 400, 800, 1200, 2000, 3000, 4000, and 5000 ms; scan time per TI: 11 min.

Stem cell labeling

PCP-Gd(acac)$_3$·2H_2O@US-tubes were used to intracellularly label pig bone-marrow-derived mesenchymal stem cells (MSCs) harvested from three different animals. To prepare the stock labeling solution, PCP-Gd(acac)$_3$·2H_2O@US-tubes were suspended in water (90 μM Gd^{3+}, by ICP-OES) and the suspension was sterilized by UV-light exposure for 3 h while rocking, which has been shown to be a procedure that does not cause damage to carbon nanotubes.[29] MSCs were grown in T-175 flasks with alpha minimal essential medium (αMEM) containing 10% fetal bovine serum (FBS) and incubated at 37 °C (95% relative humidity in 5% CO_2 in air). Cells were expanded until the third passage prior to labeling.

PCP-Gd(acac)$_3$·2H_2O@US-tubes-labeled MSCs were prepared by adding the stock labeling solution directly to the αMEM (final concentration 20 μM Gd^{3+}) followed by incubation of the cells for 24 h with the CA. After collecting the cells, the suspension was passed through a 70 μm nylon filter to eliminate cell aggregates and the cells were re-suspended in 20 mL of αMEM. A density gradient separation was performed

Open Access Article. Published on 12 June 2015. Downloaded on 12/5/2025 1:54:21 AM.
This article is licensed under a Creative Commons Attribution 3.0 Unported Licence.

in a 50 mL conical tube to isolate the cells from excess of PCP-Gd(acac)$_3$·2H$_2$O@US-tubes in solution, as well as from "heavy" cells which are labeled cells with PCP-Gd(acac)$_3$·2H$_2$O@US-tubes on their cellular membrane. To accomplish this, 10 mL of Histopaque 1077 (25 °C, Sigma-Aldrich) was added to the bottom of the conical tube containing 20 mL of the cell suspension and the sample was centrifuged at 400*g* for 20 min. The labeled MSCs were then isolated from the interface of the αMEM and the Histopaque 1077 using a plastic transfer pipette. A diagram showing this separation is shown in Fig. S5† and the effectiveness of the protocol has been demonstrated elsewhere.[4] Cells were then re-suspended in fresh αMEM and centrifuged at 1500 rpm for 10 min to wash the residue of Histopaque 1077 in cells. The cell counts were obtained using a Beckman Counter MultiSizer 3. Unlabeled MSCs were used as control cells.

Concentration of PCP-Gd(acac)$_3$·2H$_2$O@US-tubes within the MSCs

Aliquots of labeled and unlabeled (control) cell suspensions were collected in glass vials and analyzed by inductively-coupled plasma mass spectrometry (ICP-MS, using a Perkin-Elmer Inc., Elan 9000 instrumentation) to determine the Gd^{3+}-ion concentration within the cells. To prepare the samples, cells were heated and treated with two alternating additions of 500 μL 70% trace metal-grade HNO_3 and 26% $HClO_3$, allowing the samples to dry between additions. Finally, the samples were diluted to 5 mL with 2% trace metal-grade $HNO_{3(aq)}$ and filtered through a 0.22 μm pore size syringe filter.

Viability of the labeled MSCs

Fluorescence-activated cell sorting (FACS) was performed using a BD Biosciences LSRII Analyzer in order to determine the viability of the MSCs after being labeled with PCP-Gd(acac)$_3$·2H$_2$O@US-tubes for 24 h. A LIVE/DEAD viability/cytotoxicity assay kit (Life Technologies) was used to stain the cells: green-fluorescent calcein-AM indicated intracellular esterase activity in viable cells, while red-fluorescent ethidium homodimer-1 activated was to indicate dead cells when the cell membrane was compromised. Unlabeled MSCs were used as the positive control while unlabeled MSCs incubated with 70% methanol for 15 min were used as the negative control (dead cells). The dyes were added and samples were incubated in the dark at room temperature for 20 min prior to analysis.

MR imaging of labeled MSCs

PCP-Gd(acac)$_3$·2H$_2$O@US-tubes-labeled MSCs were prepared as described above. Samples of 10 million and 30 million unlabeled and labeled MSCs were separately centrifuged to form cell pellets. The supernatant was carefully removed without disturbing the cell pellet. Cautiously, cells were re-suspended in 500 μL of 0.5% agar avoiding bubble formation and transferred into a 1.5 mL eppendorf tube. The T_1-weighted MR images of the labeled and unlabeled MSCs were measured at RT using commercial 1.5 T MRI scanner (Achieva, Philips Medical System, The Netherlands) with an inversion recovery prepared spin echo sequence. Acquisition voxel size: 1.1 × 1.1 × 5 mm^3; TR/TE: 6000 ms /11 ms. The experiment was repeated at various inversion times (TIs): 50, 100, 200, 400, 600, 800, 1000, 1200, 1500, 2000, 2500, 3000, and 3500 ms. Scan time per TI: 7:30 min.

Transmission electron microscopy (TEM) imaging of the labeled MSCs

TEM analysis was performed to determine the subcellular localization of the PCP-Gd(acac)$_3$·2H$_2$O@US-tube CA. Labeled MSCs and unlabeled MSCs were centrifuged separately at 1500 rpm for 10 min to form a cell pellet. Without disturbing the pellet, the supernatant was removed and 3% glutaraldehyde was added and samples were left undisturbed for 2 days. Later, samples were washed with 1× phosphate buffered saline (PBS) and post-fixed with 1% OsO_4 for 1 h and then washed and dehydrated with increasing concentration of ethanol, and infiltrated with acetone and Epon 812 resin. Finally, samples were embedded with 100% Epon 812 in a mold and cut into 1 mm sections and stained with 1% methylene blue and 1% basic fuchsin. Ultra-thin sections of 80 nm were cut from the sample block using a Leica EM UC7 ultra microtome and framed on 100-mesh copper grids. Grids were stained with 2% alcoholic uranyl acetate and Reynold's lead citrate. The grids were examined using a JEOL 1230 TEM instrument equipped with an AMTV 600 digital imaging system at the Texas Heart Institute (Houston, TX).

Acknowledgements

A. G., M. H. R., Y. M., J. J. L., and L. J. W. acknowledge The Welch Foundation (C-0627) and the NSF Graduate Research Fellowship Program (GRFP) 0940902 (J.J.L.) for partial support of this work. The authors thank Allan Prejusa for flow cytometry analysis and Ralph Nichols for acquiring the TEM images (Texas Heart Institute at St. Luke's Episcopal Hospital, Houston, TX, USA), and Dr. Maximillian Buja (University of Texas Health Science Center of Houston, Houston, TX, USA) for his assistance with TEM analysis. The X-ray absorption spectroscopy work was carried out at the DuPont-Northwestern-Dow-Collaborative Access Team (DND-CAT) beamline at the Advanced Photon Source. the DND-CAT was supported by E.I. DuPont de Nemours & Co., the Dow Chemical Company and the State of Illinois. Use of the APS was supported by the U. S. Dept. of Energy, Office of Science, Office of Basic Energy Sciences, under Contract no. DE-AC02-06CH11357.

Notes and references

1 L. Li, W. Jiang, K. Luo, H. Song, F. Lan, Y. Wu and Z. Gu, *Theranostics*, 2013, **3**, 595–615.
2 A. Gizzatov, J. Key, S. Aryal, J. Ananta, A. Cervadoro, A. L. Palange, M. Fasano, C. Stigliano, M. Zhong, D. Di Mascolo, A. Guven, E. Chiavazzo, P. Asinari, X. Liu,

 This journal is © The Royal Society of Chemistry 2015

Open Access Article. Published on 12 June 2015. Downloaded on 12/5/2025 1:54:21 AM.
This article is licensed under a Creative Commons Attribution 3.0 Unported Licence.

M. Ferrari, L. J. Wilson and P. Decuzzi, *Adv. Funct. Mater.*, 2014, **24**, 4584–4594.
3 Y. Liu and N. Zhang, *Biomaterials*, 2012, **33**, 5363–5375.
4 L. A. Tran, R. Krishnamurthy, R. Muthupillai, M. da Graça Cabreira-Hansen, J. T. Willerson, E. C. Perin and L. J. Wilson, *Biomaterials*, 2010, **31**, 9482–9491.
5 M. Mahmoudi, H. Hosseinkhani, M. Hosseinkhani, S. Boutry, A. Simchi, W. S. Journeay, K. Subramani and S. Laurent, *Chem. Rev.*, 2011, **111**, 253–280.
6 A. A. Hassan, B. T.-Y. Chan, L. A. Tran, K. B. Hartman, J. S. Ananta, Y. Mackeyev, L. Hu, R. G. Pautler, L. J. Wilson and A. V. Lee, *Contrast Media Mol. Imaging*, 2010, **5**, 34–38.
7 R. Sethi, Y. Mackeyev and L. J. Wilson, *Inorg. Chim. Acta*, 2012, **393**, 165–172.
8 A. Gizzatov, C. Stigliano, J. S. Ananta, R. Sethi, R. Xu, A. Guven, M. Ramirez, H. Shen, A. Sood, M. Ferrari, L. J. Wilson, X. Liu and P. Decuzzi, *Cancer Lett.*, 2014, **352**, 97–101.
9 K. N. Raymond and V. C. Pierre, *Bioconjugate Chem.*, 2005, **16**, 3–8.
10 *The essential physics of medical imaging*, ed. and J. T. Bushberg, Lippincott Williams & Wilkins, Philadelphia, 2nd edn, 2002, pp. 389–391.
11 M. L. Matson and L. J. Wilson, *Future Med. Chem.*, 2010, **2**, 491–502.
12 D. Zhu, F. Liu, L. Ma, D. Liu and Z. Wang, *Int. J. Mol. Sci.*, 2013, **14**, 10591–10607.
13 B. Sitharaman, K. R. Kissell, K. B. Hartman, L. A. Tran, A. Baikalov, I. Rusakova, Y. Sun, H. A. Khant, S. J. Ludtke, W. Chiu, S. Laus, É. Tóth, L. Helm, A. E. Merbach and L. J. Wilson, *Chem. Commun.*, 2005, 3915–3917.
14 A. Gizzatov, V. Keshishian, A. Guven, A. M. Dimiev, F. Qu, R. Muthupillai, P. Decuzzi, R. G. Bryant, J. M. Tour and L. J. Wilson, *Nanoscale*, 2014, **6**, 3059–3063.
15 A. H. Hung, M. C. Duch, G. Parigi, M. W. Rotz, L. M. Manus, D. J. Mastarone, K. T. Dam, C. C. Gits, K. W. MacRenaris, C. Luchinat, M. C. Hersam and T. J. Meade, *J. Phys. Chem. C*, 2013, **117**, 16263–16273.
16 E. Bull, S. Y. Madani, R. Sheth, A. Selfalian, M. Green and A. M. Selfalian, *Int. J. Nanomedicine*, 2014, **9**, 1641–1653.
17 C. Liang, C. Wang and Z. Liu, *Part. Part. Syst. Charact.*, 2013, **30**, 1006–1017.
18 A. Bhirde, J. Xie, M. Swierczewska and X. Chen, *Nanoscale*, 2011, **3**, 142–153.
19 L. A. Tran, M. Hernández-Rivera, A. N. Berlin, Y. Zheng, L. Sampaio, C. Bové, M. da Graça Cabreira-Hansen, J. T. Willerson, E. C. Perin and L. J. Wilson, *Biomaterials*, 2014, **35**, 720–726.
20 M. Rodriguez-Porcel, *Curr. Cardiol. Rep.*, 2010, **12**, 51–58.
21 A. Gizzatov, A. Dimiev, Y. Mackeyev, J. M. Tour and L. J. Wilson, *Chem. Commun.*, 2012, **48**, 5602–5604.
22 J. J. Law, A. Guven and L. J. Wilson, *Contrast Media Mol. Imaging*, 2014, **9**, 409–412.
23 J.-P. Korb, *J. Chem. Phys.*, 1983, **78**, 5782–5789.
24 J.-P. Korb, M. Whaley-Hodges and R. Bryant, *Phys. Rev. E: Stat., Nonlinear, Soft Matter Phys.*, 1997, **56**, 1934–1945.
25 J.-P. Korb, A. Delville, S. Xu, G. Demeulenaere, P. Costa and J. Jonas, *J. Chem. Phys.*, 1994, **101**, 7074–7081.
26 R. Sethi, Ph.D. Dissertation, Rice University, 2013.
27 P. Cherukuri, C. J. Gannon, T. K. Leeuw, H. K. Schmidt, R. E. Smalley, S. A. Curley and R. B. Weisman, *Proc. Natl. Acad. Sci. U. S. A.*, 2006, **103**, 18882–18886.
28 Z. Gu, H. Peng, R. H. Hauge, R. E. Smalley and J. L. Margrave, *Nano Lett.*, 2002, **2**, 1009–1013.
29 S. Bellucci, M. Chiaretti, P. Onorato, F. Rossella, M. S. Grandi, P. Galinetto, I. Sacco and F. Micciulla, *Nanomed.*, 2010, **5**, 209–215.